Bulletin of Electrical Engineering and Informatics
Vol. 15, No. 1, February 2026, pp. 277~289
ISSN: 2302-9285, DOI: 10.11591/eei.v15i1.10734

Performance analysis of rate-splitting multiple access in multi-RIS-assisted wireless communication

Hong-Nhu Nguyen[1], Xuan-Tien Nguyen[1], Sang-Quang Nguyen[2]
[1]Faculty of Technology and Engineering, Saigon University (SGU), Ho Chi Minh City, Vietnam
[2]Wireless Communication Laboratory, Posts and Telecommunications Institute of Technology, Ho Chi Minh City, Vietnam

Article Info

Article history:

Received May 22, 2025
Revised Oct 30, 2025
Accepted Dec 6, 2025

Keywords:

Gamma distribution
Multi-reconfigurable intelligent surface
Outage probability
Rate-splitting multiple access
Reconfigurable intelligent surfaces
Throughput

ABSTRACT

This paper presents a novel rate-splitting multiple access (RSMA) framework with partial reconfigurable intelligent surface (PRIS) selection over Nakagami-*m* fading channels, a scenario that has not been comprehensively analyzed in prior works. To this end, we conduct a detailed performance analysis of a wireless communication system that incorporates multiple reconfigurable intelligent surfaces (RISs) as cooperative relays. The proposed framework integrates RSMA with a PRIS selection strategy, enabling efficient data transmission from the base station (BS) to two users with distinct channel conditions. Closed-form expressions for the outage probability and achievable throughput are derived over independent and non-identically distributed (i.n.i.d.) Nakagami-*m* fading channels. The analysis highlights the role of PRIS in enhancing system efficiency and ensuring fair resource allocation between users. In addition, asymptotic evaluations offer deeper insights into the system's behavior under varying channel dynamics. Simulation results are provided to validate the theoretical findings, demonstrating a close match with the analytical expressions and confirming the robustness of the proposed approach.

Corresponding Author:

Sang-Quang Nguyen
Wireless Communication Laboratory, Posts and Telecommunications Institute of Technology
Ho Chi Minh City, Vietnam
Email: sangnq@ptit.edu.vn

1. INTRODUCTION

The sixth-generation (6G) wireless network is envisioned as a foundational infrastructure for next-generation communication systems, aiming to deliver ultra-high reliability, low latency, massive connectivity, and energy efficiency [1]–[3]. Among various enabling technologies, reconfigurable intelligent surfaces (RISs) have recently drawn significant research attention for their ability to dynamically control electromagnetic waves to enhance wireless signal propagation [4], [5]. By intelligently reflecting incident signals, RIS can effectively extend coverage, mitigate fading, and improve both spectral and energy efficiency. Furthermore, RIS-assisted systems have demonstrated promising enhancements in physical layer security (PLS), especially when integrated with non-orthogonal multiple access (NOMA) to combat eavesdropping threats and ensure confidentiality [6], [7].

To further improve system performance and coverage, multiple distributed RIS deployments have been proposed as passive relays to overcome obstacles such as blocked line-of-sight (LoS) links [8], [9]. Advanced RIS technologies like simultaneously transmitting and reflecting RIS (STAR-RIS) further expand coverage and improve outage performance, even under imperfect channel state information (CSI) [10]. These multi-RIS-assisted architectures find practical relevance in complex environments including smart cities, high-speed transportation, and industrial IoT settings [11].

Simultaneously, advanced multiple access schemes such as rate-splitting multiple access (RSMA) have emerged as powerful alternatives to conventional orthogonal multiple access (OMA) and NOMA. RSMA splits user messages into common and private parts, offering robustness against CSI imperfections and interference [12], [13]. Despite these advantages, RSMA's integration with distributed multi-RIS setups remains underexplored. Initial studies have laid groundwork for RSMA-enabled multi-RIS systems [14], [15], but comprehensive performance analyses under generalized fading models are still lacking.

Additionally, many prior works assume idealized fading models such as Rayleigh or Rician channels, which may not accurately capture diverse real-world propagation scenarios. Nakagami-*m* fading offers a more general and flexible model to characterize varying multipath severities [16], [17]. As the scale of RIS deployments grows, activating all RIS units simultaneously leads to excessive system overhead and complexity. Consequently, RIS selection strategies like opportunistic RIS-aided (ORA) and exhaustive RIS-aided (ERA) schemes have been proposed to balance performance and complexity [18], [19]. Partial RIS selection (PRIS), which aims to further optimize this trade-off, remains relatively unexplored.

Beyond these challenges, emerging applications such as online gaming, extended reality (XR), metaverse, and industrial IoT require ultra-reliable and low-latency communications (URLLC) coupled with stringent security and privacy guarantees. Short-packet communication (SPC) has become essential for meeting URLLC demands. Recent works integrating RIS, NOMA, and SPC have introduced novel user-pairing and phase-shift design methods to protect digital content and copyrights from untrusted users, enhancing secure short-packet transmission in these emerging scenarios [20]. Although RSMA and RIS have been extensively studied in isolation, their integration under generalized Nakagami-*m* fading channels with partial RIS selection has not been comprehensively analyzed. This knowledge gap motivates the present work. Beyond static and moderately mobile cases, future 6G networks must also support users with high mobility (e.g., vehicular and high-speed rail) as well as those located at the cell edge with poor channel conditions. Both scenarios pose significant challenges in terms of reliable coverage and quality-of-service. By intelligently combining RSMA and PRIS in a multi-RIS-assisted architecture, the proposed framework is particularly well-suited to enhance robustness for highly mobile users and to extend coverage for cell-edge users.

To address these limitations, this paper proposes a novel cooperative communication system that integrates RSMA and PRIS in a multi-RIS-assisted framework. Our key contributions are summarized as follows:

a. We design a multi-RIS-assisted communication framework where a base station (BS) serves two users located beyond its direct coverage, utilizing RISs as passive relays. Closed-form expressions for outage probability and achievable throughput are derived over independent and non-identically distributed (i.n.i.d.) Nakagami-*m* fading channels.
b. We perform asymptotic analysis to reveal the impact of critical system parameters-including the number of RISs, power allocation (PA) coefficients, and the number of reflection elements per RIS–on system reliability and user fairness.
c. Simulation results validate the analytical expressions and demonstrate that the proposed scheme significantly outperforms conventional NOMA under various practical configurations.
d. Table 1 compares our work with existing literature, highlighting the novelty and comprehensiveness of our analysis.

Table 1. Comparison of our work with existing literature

Ref./prop.	Multi-RIS	RSMA	Nakagami-*m* fading	Outage probability	Asymptotic analysis	Throughput
[1]	✗	✗	✗	✓	✓	✓
[18]	✗	✗	✓	✗	✓	✗
[19]	✓	✗	✓	✗	✓	✗
[14]	✓	✓	✗	✓	✗	✗
[15]	✗	✓	✗	✓	✗	✗
Proposed work	✓	✓	✓	✓	✓	✓

The remainder of this paper is structured as follows. Section 2 introduces the system model. Section 3 presents the performance analysis. Section 4 discusses simulation results. Finally, section 5 concludes the paper.

2. SYSTEM MODEL AND CHANNEL CHARACTERISTICS

2.1. System description

Figure 1 depicts the wireless communication framework under consideration, which includes a BS outfitted with a single transmit antenna, alongside two users (D_1 and D_2), each possessing a single receive antenna. It is posited that there are obstructions between the BS and both D_1 and D_2, thereby preventing the BS from directly transmitting signals to these users. Each RIS comprises Nm reflective elements. For the purpose of simplification, we will consider that all M RIS units are homogeneous, such that $N = N_1 = N_2 = \cdots = N_M$. In accordance with the findings presented in [21], it is assumed that complete channel state information (CSI) is accessible. The communication sequence initiates with the BS delivering the signal to the mth RIS ($(m = 1,2, \dots, M)$), which subsequently reflects the signal in a passive manner towards D_1 and D_2. To achieve this, the mth RIS (denoted as RIS$_m$ for brevity) fine-tunes the phase reflection coefficient to enhance the received signal-to-interference-plus-noise ratio (SINR) at both D_1 and D_2, thereby improving the overall end-to-end quality of the communication system. We assume that the channels undergo independent Nakagami-m fading.

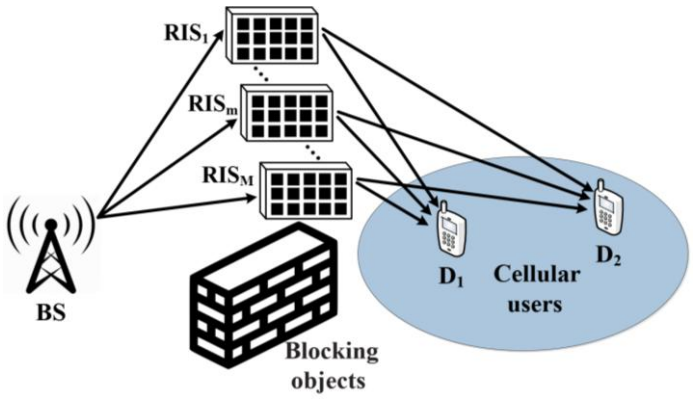

Figure 1. System model

Initially, the BS categorizes the messages from cellular users (CUs) into common and private components. Subsequently, it encodes all common components into a singular stream denoted as x_c, while encoding the private components into distinct individual streams represented as x_k, $k \in \{1,2\}$. It is established that $E\{|x_c|^2\} = E\{|x_k|^2\} = 1$. Let P_S signify the transmission power of the BS, which is allocated with PA factors a_c and a_k corresponding to x_c and x_k, respectively, such that $a_c + \sum_{k=1}^{2} a_k = 1$. Consequently, each user receives a mix of these messages from BS, provided by (1):

$$x = \sqrt{P_S a_c}\, x_c + \sum_{k=1}^{2} \sqrt{P_S a_k}\, x_k \tag{1}$$

Here, a_c and a_k are the PA coefficients for the common and private streams, respectively, and all streams are normalized to unit power. In the RSMA framework, the common stream x_c and the private streams x_k are multiplexed into a single transmitted signal as expressed in (1). Accordingly, each user receives a superposition of the common and private components, along with interference and noise. This guarantees consistency with the received signal model in (2), where each user first decodes the common stream and then its own private stream after applying successive interference cancellation (SIC). The overall signal is transmitted from the BS to the mth RIS, denoted as RIS$_m$, and then passively reflected toward both users. Consequently, the received signal at user $D_k (k \in \{1,2\})$ can be expressed as (2):

$$\bar{y}_{D_k}^{m} = \left[\sum_{q=1}^{N} h_{mq}\, g_{mq,k} e^{j\phi_{mq}^{k}}\right] x + \bar{\omega}_{D_k}^{m} = \underbrace{\left[\sum_{q=1}^{N} h_{mq}\, g_{mq,k} e^{j\phi_{mq}^{k}}\right] \sqrt{P_S a_c}\, x_c}_{\text{Commonmessage}} +$$
$$\underbrace{\left[\sum_{q=1}^{N} h_{mq}\, g_{mq,k} e^{j\phi_{mq}^{k}}\right] \sqrt{P_S a_k}\, x_k}_{\text{Desiredprivatemessage}} + \underbrace{\left[\sum_{q=1}^{N} h_{mq}\, g_{mq,k} e^{j\phi_{mq}^{k}}\right] \sqrt{P_S a_i}\, x_i}_{\text{Interference}} + \underbrace{\bar{\omega}_{D_k}^{m}}_{\text{AWGN}} \tag{2}$$

where $k \in \{1,2\}, i \in \{2,1\}, k \neq i$. Here, $g_{mq,1}$ and $g_{mq,2}$ denote the channel coefficients of the BS $\rightarrow$ RIS$_m$, RIS$_m$ $\rightarrow D_1$, and RIS$_m$ $\rightarrow D_2$ links, respectively. In Table 2, these coefficients are modeled as:

$h_{mq} = d_{SR_m}^{-\delta/2}\alpha_{mq}e^{-j\theta_{mq}}, g_{mq,k} = d_{R_mD_k}^{-\delta/2}\beta_{mq,k}e^{-j\varepsilon_{mq,k}}$, where d_{SR_m} and $d_{R_mD_k}$ denote the respective link distances, δ is the path-loss exponent, and α_{mq}, $\beta_{mq,k}$ are the amplitude fading parameters. The phases θ_{mq} and $\varepsilon_{mq,k}$ represent the corresponding phase shifts due to fading. The additive noise terms follow circularly symmetric complex Gaussian distributions, such that $\text{RIS}_m \rightarrow \bar{\omega}_{D_k}^{m} \sim \mathcal{CN}(0, \omega_{D_k}^2)D_2$.

Table 2. Summary of notations

Symbol	Description
P_S	Total transmit power of the BS
a_c, a_k	PA coefficients for common and private streams ($a_c + \sum_k a_k = 1$)
M	Number of RISs; N: number of reflecting elements per
d_{SR_m}	Distance from BS to the mth RIS
$d_{R_mD_k}$	Distance from RIS_m to user D_k
δ	Path-loss exponent
$\alpha_{mq}, \beta_{mq,k}$	Nakagami-m fading amplitudes for BS–RIS and RIS–user links
$\omega_{D_k}^2$	Noise power at user D_k; $\rho_S = P_S/\omega_{D_k}^2$
ζ_k	Large-scale loss term $d_{SR_m}^{\delta} d_{R_mD_k}^{\delta}$

Following the assumption in [21], we consider that RISm has perfect knowledge of the channel state information (CSI), including h_{mq} and $g_{mq,k}$. According to Vu *et al*. [22], RSMA systems employ successive interference cancellation (SIC) to decode user-specific signals. Each user first decodes the common message by treating all private signals as interference. The corresponding signal-to-interference-plus-noise ratio (SINR) for decoding the common message at user D_k is given by (3):

$$\bar{\gamma}_{k,x_c}^{m} = \frac{a_c P_S \left|\sum_{q=1} \alpha_{mq}\beta_{mq,k} e^{j(\phi_{mq}^{k} - \theta_{mq} - \varepsilon_{mq,k})}\right|^2}{a_k P_S \left|\sum_{q=1} \alpha_{mq}\beta_{mq,k} e^{j(\phi_{mq}^{k} - \theta_{mq} - \varepsilon_{mq,k})}\right|^2 + \zeta_k \omega_{D_k}^2}, \tag{3}$$

where $\zeta_k = d_{SR_m}^{\delta} d_{R_mD_k}^{\delta}$ the phase shift ϕ_{mq}^{k} is adjusted to align with the total phase of the channel. Specifically, to maximize the received signal power, each reflecting element is configured such that: $\phi_{mq}^{k} = \theta_{mq} + \varepsilon_{mq,k}, \forall q, m$.

This phase alignment is a common assumption in RIS literature (e.g., [14], [21], [23]–[25]) and allows for coherent signal combining. Substituting this into (3) yields the optimized SINR:

$$\bar{\gamma}_{k,x_c}^{m} = \frac{a_c P_S |A_k|^2}{a_k P_S |A_k|^2 + \zeta_k \omega_{D_k}^2} \frac{a_c \rho_S |A_k|^2}{a_k \rho_S |A_k|^2 + \zeta_k}, \tag{4}$$

where $\rho_S = \frac{P_S}{\omega_{D_k}^2}$ is so-called the average signal-to-noise ratio (SNR) and $A_k \triangleq \left|\sum_{q=1}^{N} \alpha_{mq}\beta_{mq,k}\right|$. It is important to acknowledge that$x_c$and$x_k$represent normalized unity power signals, specifically characterized by the properties $\mathbb{E}\{|x_c|^2\} = \mathbb{E}\{|x_k|^2\} = 1$, where $\mathbb{E}\{\cdot\}$ signifies the expectation operator. Upon the successful interpretation of the shared message, the subsequent phase requires each user to decipher their intended private message by deducting the decoded common message from the received signal, while presuming that the private messages of all other users serve as interference. The SINR for the kth user to decode the private message can be articulated as (5):

$$\bar{\gamma}_{k,x_k}^{m} = \frac{a_k \rho_S |A_k|^2}{a_i \rho_S |A_k|^2 + \zeta_k}, \quad (i \neq k). \tag{5}$$

Here, $A_k = \sum_{q=1}^{N} \alpha_{mq}\, \beta_{mq,k}$ denotes the coherent sum of fading amplitudes for user D_k. This notation is used consistently in (4) and (5) and throughout the subsequent derivations.

Intuition for (3)–(5). In (3), the numerator represents the coherently combined desired signal power obtained under perfect CSI, while the denominator comprises inter-user interference and noise when decoding the *common* stream. After successive interference cancellation (SIC), (5) describes the *private* decoding stage where the desired private signal remains in the numerator and the residual inter-user interference plus noise is in the denominator. This two-stage decoding (common → private) captures the essence of RSMA and explains the performance/fairness gains observed later.

Modeling assumptions. For analytical tractability, we consider single-antenna BS and two single-antenna users; RISs are homogeneous with $N_1 = \cdots = N_M = N$ and operate in passive reflection mode. All links (BS→RIS$_m$ and RIS$_m$ →D_k) follow independent but non-identically distributed Nakagami-m fading; AWGN at D_k has variance $\omega_{D_k}^2$. Consistent with common practice in RIS studies, perfect CSI is assumed at the BS and at RISs to enable phase alignment for coherent combining (cf. (3)–(5)).
Feasibility of PRIS. In practice, PRIS can be implemented with low-complexity measurements and selection. Each RIS (or the BS) collects a lightweight quality metric per user (e.g., pilot-based received strength or an SINR proxy) and selects the RIS that maximizes the criterion in (14). This incurs complexity on the order of the number of RIS panels M (one metric per panel), in contrast to full activation that scales with both M and N. Hence, PRIS reduces control/estimation overhead and power consumption, making it attractive for real-time and scalable deployments.

2.2. Channel characteristics

Under Nakagami-m fading, the probability density function (PDF) and cumulative distribution function (CDF) of a channel coefficient $W \in \{\alpha_{mq}, \beta_{mq,1}, \beta_{mq,2}\}$ are given by [26]:

$$f_{|W|}(x) = \frac{2}{\Gamma(m_W)}\left(\frac{m_W}{\Omega_W}\right)^{m_W} x^{2m_W-1}\, exp\left(-\frac{m_W x^2}{\Omega_W}\right), \tag{6a}$$

$$F_{|W|}(x) = \frac{\gamma\left(m_W, \frac{m_W}{\Omega_W}x^2\right)}{\Gamma(m_W)}, \tag{6b}$$

where $\Gamma(\cdot)$ denotes the complete Gamma function, $\gamma(\cdot,\cdot)$ is the lower incomplete Gamma function, m_W is the shape parameter, and $\Omega_W > 0$ represents the average channel power.

Let us define the product of two independent Nakagami-m variables as $Z_{Q_{mq,k}} = |\alpha_{mq}||\beta_{mq,k}|$, for $k \in \{1,2\}$. Its PDF can be computed via:

$$f_{Z_{Q_{mq,k}}}(x) = \int_0^\infty \frac{1}{y} f_{\alpha_{mq}}(y) f_{\beta_{mq,k}}\left(\frac{x}{y}\right) dy. \tag{7}$$

Using (6a) and [27, (3.471.9)], the closed-form expression for $f_{Z_{Q_{mq,k}}}(x)$ is obtained as (8):

$$f_{Z_{Q_{mq,k}}}(x) = \frac{4x^{m_\alpha + m_{\beta_k} - 1}}{\Gamma(m_\alpha)\Gamma(m_{\beta_k})}\left(\sqrt{\frac{m_\alpha m_{\beta_k}}{\Omega_\alpha \Omega_{\beta_k}}}\right)^{m_\alpha + m_{\beta_k}} \times K_{m_\alpha - m_{\beta_k}}\left(2\sqrt{\frac{m_\alpha m_{\beta_k}}{\Omega_\alpha \Omega_{\beta_k}}}x\right), \tag{8}$$

where $m_\alpha = m_{\alpha_{mq}}, m_{\beta_k} = m_{\beta_{mq,k}}$, and $K_a(\cdot)$ is the modified Bessel function of the second kind and order a. The kth moment of $Z_{Q_{mq,k}}$, denoted by $\mu_{Z_{Q_{mq,k}}}(k) = \mathbb{E}[Z_{Q_{mq,k}}^k]$, can be derived using [27, (6.561.16)]:

$$\mu_{Z_{Q_{mq,k}}}(k) = \frac{\Gamma(m_\alpha + 0.5k)\Gamma(m_{\beta_k} + 0.5k)}{\Gamma(m_\alpha)\Gamma(m_{\beta_k})}\left(\frac{\Omega_\alpha \Omega_{\beta_k}}{m_\alpha m_{\beta_k}}\right)^{0.5k}. \tag{9}$$

From (6a) and (6b) make it difficult to derive the expression closed-form of $Z_{Q_{mq,k}}$, we may alter it to the Gamma distribution. The PDF and CDF of $Q_{mq,k}$ are presented as (10a) and (10b):

$$f_{Q_{mq,k}}(x) \approx \frac{\phi_k^{\varphi_k} x^{\varphi_k - 1}}{\Gamma(\varphi_k)} e^{-\phi_k x}, \tag{10a}$$

$$F_{Q_{mq,k}}(x) \approx \frac{\gamma(\varphi_k, \phi_k x)}{\Gamma(\varphi_k)}, \tag{10b}$$

In which

$$\varphi_k = \frac{N\left(\mu_{Z_{Q_{mq,k}}}(1)\right)^2}{\mu_{Z_{Q_{mq,k}}}(2) - \left(\mu_{Z_{Q_{mq,k}}}(1)\right)^2}, \tag{11a}$$

$$\phi_k = \frac{\mu_{Z_{Q_{mq,k}}}{}^{(1)}}{\mu_{Z_{Q_{mq,k}}}{}^{(2)} - \left(\mu_{Z_{Q_{mq,k}}}{}^{(1)}\right)^2}, \tag{11b}$$

where $\mathbb{E}[\cdot]$, $\mathrm{Var}[\cdot]$ denote the expectation and variance, respectively.

To derive the distribution of squared amplitudes, consider the transformation $X = Y^2$ for a random variable Y. Then, its distribution becomes $F_X(x) = F_Y(\sqrt{x})$, and $f_X(x) = \frac{1}{2\sqrt{x}} f_Y(\sqrt{x})$. Applying this transformation to the Gamma-approximated $Q_{mq,k}$, the PDF and CDF of $|\mathcal{A}_k|^2$ can be expressed as (12) and (13):

$$f_{|\mathcal{A}_k|^2}(x) = \frac{\phi_k^{\varphi_k}}{2\Gamma(\varphi_k)} x^{0.5(\varphi_k-2)}\, exp(-\phi_k\sqrt{x}), \tag{12}$$

$$F_{|\mathcal{A}_k|^2}(x) = \frac{\gamma(\varphi_k, \phi_k\sqrt{x})}{\Gamma(\varphi_k)}. \tag{13}$$

3. PERFORMANCE ANALYSIS

This section provides a detailed examination of the system's performance in terms of outage probability (OP), asymptotic behavior, and throughput. To streamline the analysis, we assume that a single RIS among the M available RISs is selected to support the transmission. The selected RIS is the one that maximizes the signal reception quality at the target destination. Accordingly, the optimal RIS selection criteria are defined as (14a) and (14b):

$$m_1^* = argmax \quad_{m_1 \in \{1,2,\ldots,M\}} (\bar{\gamma}_1^m < 1), \tag{14a}$$

$$m_2^* = argmax \quad_{m_2 \in \{1,2,\ldots,M\}} (\bar{\gamma}_2^m < 1), \tag{14b}$$

where $\bar{\gamma}_1^m = min\left(\frac{\bar{\gamma}_{1,x_c}^m}{\varepsilon_c}, \frac{\bar{\gamma}_{1,x_1}^m}{\varepsilon_1}\right), \bar{\gamma}_2^m = min\left(\frac{\bar{\gamma}_{2,x_c}^m}{\varepsilon_c}, \frac{\bar{\gamma}_{2,x_2}^m}{\varepsilon_2}\right)$ with threshold parameters defined as $\varepsilon_c = 2^{R_c} - 1, \varepsilon_1 = 2^{R_1} - 1, \varepsilon_2 = 2^{R_2} - 1$. In which R_c, R_1, and R_2 are the target data rates for decoding signals x_c, x_1, and x_2 at users D_1 and D_2, respectively.

We provide a compact flowchart of the derivations in Figure 2 to guide the reader from the channel model to the closed forms, asymptotic, and throughput.

Analytical pipeline: 1) Channel/statistical model (i.n.i.d. Nakagami-*m*) → 2) Effective SINR expressions (3)–(5) under perfect CSI → 3) PRIS selection criterion (14) → 4) Outage probability definitions and closed-form expressions → 5) Asymptotic (high-SNR) behavior → 6) Throughput computation via rate averaging.

Figure 2. Flow of the analytical derivations

Based on the order statistics of independent and identically distributed (i.i.d.) fading links, the CDFs of the selected SINRs $\bar{\gamma}_1^{m_1^*-}$ and $\bar{\gamma}_2^{m_2^*}$ can be expressed as (15a) and (15b):

$$F_{\bar{\gamma}_1^{m_1^*}}(x) = \left[F_{\bar{\gamma}_1^m}(x)\right]^M, \tag{15a}$$

$$F_{\bar{\gamma}_2^{m_2^*}}(x) = \left[F_{\bar{\gamma}_2^m}(x)\right]^M. \tag{15b}$$

This produces the PDF displayed in (16a) and (16b):

$$f_{\bar{\gamma}_1^{m_1^*}}(x) = M f_{\bar{\gamma}_1^m}(x)\left[F_{\bar{\gamma}_1^m}(x)\right]^{M-1}, \tag{16a}$$

$$f_{\bar{\gamma}_2^{m_2^*}}(x) = M f_{\bar{\gamma}_2^m}(x)\left[F_{\bar{\gamma}_{2,x_2}^m}(x)\right]^{M-1}. \tag{16b}$$

3.1. Outage probability analysis

In signaling based on RSMA, every user obtains a mix of a common message and their private message, along with the private messages from all other users, and processes both messages using a two-step decoding approach, as outlined in (4) and (5). Should these SINRs drop below the required thresholds $\varepsilon_c$and ε_k, respectively, the connection between the BS-RIS$_m$ and the kth user will experience an outage.

For user k, an outage occurs when either the common-stream or the private-stream SINR falls below its target. Equivalently, $\mathcal{P}_{D_k} = Pr\left\{min\ (\bar{\gamma}_{k,xc}/\varepsilon_c,\ \bar{\gamma}_{k,xk}/\varepsilon_k) < 1\right\}$. This form makes explicit that both decoding stages must be simultaneously supported. Using the PRIS rule in (14a) and (14b), the closed-form expression is then obtained in (17).

The link between BS-RIS$_m$ and the kth user has an outage probability that is determined by (17):

$$\mathcal{P}_{D_k} = \begin{cases} \left[\frac{1}{\Gamma(\varphi_k)}\gamma\left(\varphi_k, \phi_k\sqrt{\frac{\varepsilon_c}{\rho_S(a_c - a_k\varepsilon_c)}}\right)\right]^M & \hat{\varepsilon}_c \geq \hat{\varepsilon}_k \\ \left[\frac{1}{\Gamma(\varphi_k)}\gamma\left(\varphi_k, \phi_k\sqrt{\frac{\varepsilon_k}{\rho_S(a_k - a_i\varepsilon_k)}}\right)\right]^M & \hat{\varepsilon}_c \leq \hat{\varepsilon}_k \end{cases} \quad (17)$$

where $k \in \{1,2\}, i \in \{2,1\}, k \neq i$, $\hat{\varepsilon}_c = \frac{\varepsilon_c}{\rho_S(a_c - a_k\varepsilon_c)}$ and $\hat{\varepsilon}_k = \frac{\varepsilon_k}{\rho_S(a_k - a_i\varepsilon_k)}$.

Proof 1. By applying the selection criterion for the RIS presented in (14a) and (14b), the system attains best performance. Consequently, the outage probability for the kth user can be assessed by (18):

$$\mathcal{P}_{D_k} = Pr\left(min\left(\frac{\bar{\gamma}_{k,x_c}^{m_k^*}}{\varepsilon_c}, \frac{\bar{\gamma}_{k,x_k}^{m_k^*}}{\varepsilon_k}\right)\right) = \left[1 - Pr\left(\bar{\gamma}_{k,x_c}^{m} > \varepsilon_c, \bar{\gamma}_{k,x_k}^{m} > \varepsilon_k\right)\right]^M. \quad (18)$$

When we replace $\bar{\gamma}_{k,x_c}^{m}$ and $\bar{\gamma}_{k,x_k}^{m}$ from (4) and (5) in (18), we get:

$$\mathcal{P}_{D_k} = \left[1 - Pr\left(\frac{a_c\rho_S|A_k|^2}{(1-a_c)\rho_S|A_k|^2 + \zeta_k} > \varepsilon_c, \frac{a_k\rho_S|A_k|^2}{a_i\rho_S|A_k|^2 + \zeta_k} > \varepsilon_k\right)\right]^M. \quad (19)$$

Following a few algebraic reductions, (19) may be written as (20):

$$\mathcal{P}_{D_k} = [1 - Pr(|A_k|^2 > \hat{\varepsilon}_c, |A_k|^2 > \hat{\varepsilon}_k)]^M = \left[Pr(|A_k|^2 \leq \hat{\varepsilon}_{max}())\ []^M\left[F_{|A_k|^2}(\hat{\varepsilon}_{max}())[]^M\right]\right] \quad (20)$$

where $\hat{\varepsilon}\ max(\hat{\varepsilon}_c, \hat{\varepsilon}_k)_{max}$, $\hat{\varepsilon}_c$ and $\hat{\varepsilon}_k$ are already listed below (17). Solving (20) with (13) yields (17).

The proof is completed.

Remark on Gamma approximation. To keep the analysis tractable, the product of independent Nakagami-m amplitudes in the cascaded BS–RIS–user link is approximated via a Gamma distribution using moment matching (with parameters in (11a) and (11b)). This approximation is accurate for moderate-to-large m and independent hops, but may incur tail mismatch when $m \ll 1$ (severe fading), when the number of cascaded factors is small, or when link correlations exist. The practical impact of these edge cases is assessed through Monte Carlo validation in section 4, where the analytical curves closely follow the simulated results.

3.2. Asymptotic analysis

Using [27], we may approximate the lower incomplete Gamma function as (21):

$$\gamma\left(\varphi_k, \phi_k\sqrt{x}\right) = \frac{\left[\phi_k\sqrt{x}\right]^{\varphi_k}}{\varphi_k}, x \to 0 \quad (21)$$

From (21) into (17) and under high SNR conditions, the outage probability for the kth user can be asymptotically represented as (22):

$$\mathcal{P}_{D_k}^{\infty} = \begin{cases} \left\langle\frac{1}{\varphi_k\Gamma(\varphi_k)}\left[\phi_k\sqrt{\frac{\varepsilon_c}{\rho_S(a_c - a_k\varepsilon_c)}}\right]^{\varphi_k}\right\rangle^M & \hat{\varepsilon}_c \geq \hat{\varepsilon}_k \\ \left\langle\frac{1}{\varphi_k\Gamma(\varphi_k)}\left[\phi_k\sqrt{\frac{\varepsilon_k}{\rho_S(a_k - a_i\varepsilon_k)}}\right]^{\varphi_k}\right\rangle^M & \hat{\varepsilon}_c \leq \hat{\varepsilon}_k \end{cases} \quad (22)$$

3.3. Throughput analysis

In this subsection, we delve deeper into a metric of throughput within a delay-constrained transmission mode, focusing on outage performance. This throughput signifies the system's capability when a specific data rate is necessary. We can derive the throughput at these crucial nodes, as illustrated (23):

$$\tau_k = \left(1 - P_{D_k}\right) R_k,\ k \in \{1,2\} \tag{23}$$

3.4. Computational complexity and fairness analysis

Computational complexity: activating all RIS panels simultaneously requires optimizing $M \times N$ reflecting elements, which leads to complexity on the order of $\mathcal{O}(MN)$. In contrast, PRIS selects only the best RIS panel, reducing the burden to $\mathcal{O}(M)$ for RIS selection plus $\mathcal{O}(N)$ for phase alignment. This demonstrates that PRIS offers a scalable and practical solution with significantly lower computational cost.

Sensitivity to imperfections: in practice, channel state information (CSI) is rarely perfect, and RIS elements typically support only $L-$ bitphase quantization. Both factors may slightly degrade outage and throughput performance, especially at high SNR. However, prior works have shown that RSMA is robust against CSI uncertainty, while even coarse quantization (e.g., L=2 or 3 bits) retains most RIS gains. Therefore, the proposed PRIS strategy is expected to remain effective under realistic operating conditions. fairness evaluation: to quantify user equity, Jain's fairness index is considered:

$$J = \frac{(\sum_{k=1}^{k} R_k)^2}{K \cdot \sum_{k=1}^{k} R_k^2}, \tag{24}$$

where R_k is the throughput of user k and $K = 2$. A value of J close to 1 indicates high fairness. This metric will be reported in Section 4 to complement the outage and throughput analysis.

4. NUMERICAL RESULTS

This section presents numerical results to validate the derived theoretical expressions. The core system parameters are summarized in Table 3. Unless otherwise specified, these parameters are used throughout the simulations. The equivalent noise power at users D_1 and D_2 is computed as $\omega_{D_1}^2 = \omega_{D_2}^2 = N_0 + 10\,log\ _{10}(\text{BW}) + \text{NF}\,[\text{dBm}]$, [19]. The PA coefficients are set as $a_c = 0.8, a_1 = 0.4(1 - a_c)$, and $a_2 = 0.6(1 - a_c)$. Symbolic computation is utilized in MATLAB to enhance the precision of theoretical evaluations. To enhance the credibility of our Monte Carlo simulations, we verified that the plotted curves are consistent with the 95% confidence intervals of the empirical results. The variance was negligible due to the large number of iterations (10^6), hence error bars would visually overlap with the curves.

Table 3. Main system parameters

Parameter	Value
Monte Carlo simulations	10^6 iterations
Number of RISs	$M = 2$
Number of reflecting elements per RIS	$N = 2$
Nakagami fading parameter	$m = 1$
Target rate (common)	R_c= 0.25 bps/Hz
Target rate (D_1)	R_1= 0.5 bps/Hz
Target rate (D_2)	R_2= 0.1 bps/Hz
Bandwidth	BW = 10 MHz
Noise figure (NF)	10 dBm
Thermal noise density (N_0)	-174 dBm/Hz
Distance: BS to RIS$_m$	$d_{SR_m} = 5$ m
Distance: RIS$_m$ to D_1	$d_{SR_mD_1} = 10$ m
Distance: RIS$_m$ to D_2	$d_{SR_mD_2} = 10$ m
Path loss exponent	$\delta = 2$

Figure 3 depicts the outage probability of users D_1 and D_2 as a function of the BS transmit power PS for different numbers of reflecting elements N. Theoretical results derived from (17) are represented by square (D_1) and circle (D_2) markers, while solid lines correspond to Monte Carlo simulations. The dashed curves indicate the asymptotic expressions in (22), which closely match the simulation results at high SNR, thereby confirming the validity of the asymptotic analysis. As the number of reflecting elements N increases

from 1 to 3, a clear reduction in outage probability is observed for both users, particularly in the low-to-moderate SNR regime. This demonstrates the substantial performance gains achievable through denser RIS deployments, which enhance signal reflection diversity and overall system reliability.

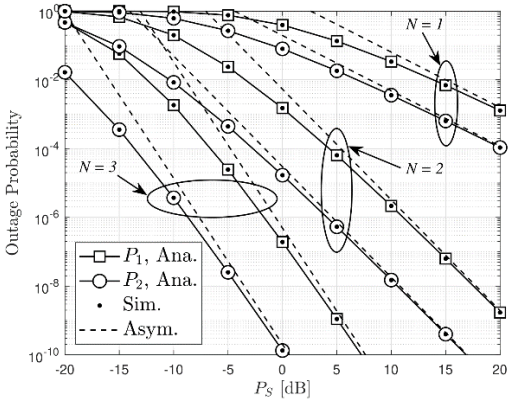

Figure 3. Outage probability versus BS transmit power P_S for different numbers of reflecting elements N

Figure 4 investigates the effects of two key parameters on the system's outage performance. In Figure 4(a), increasing the number of RISs M (with fixed $N = 2$ and $m = 1$) results in a noticeable reduction in outage probability for both users. Figure 4(b) increasing m leads to a substantial decrease in the outage probability. This is because higher m values reduce the depth and frequency of signal fades, making the channel more stable. This improvement highlights the benefit of spatial diversity achieved by deploying multiple RIS panels.

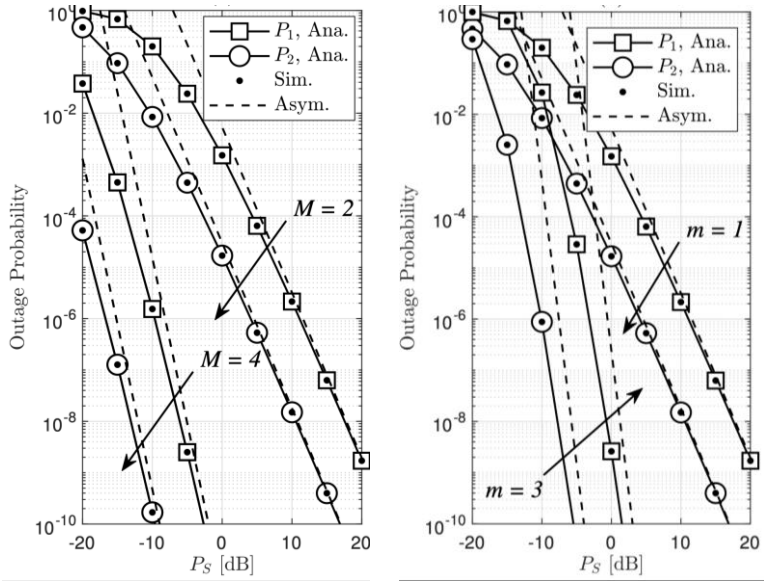

(a) (b)

Figure 4. Impact of system parameters on outage probability; (a) impact of RIS quantity M on outage probability ($N = 2, m = 1$) and (b) impact of fading parameter m on outage probability ($M = 2, N = 2$)

Figure 5 illustrates the relationship between the outage probability and the PA coefficient ac for two users P_1 and P_2 under different transmit powers $P_S = 5$ dB and $P_S = 15$ dB. The figure shows that there exists an optimal a_c (around 0.35–0.4) that minimizes outage probability for both users. When ac is too small or too large, the outage probability increases significantly, indicating poor power distribution. As P_S increases, the overall outage performance improves and the performance gap between different a_c value

narrows, highlighting the importance of optimal PA in RSMA for maintaining user fairness and system efficiency.

Figure 6 investigates the effect of the distance dSRm between the BS and RIS$_m$ on the outage probability. As d_{SR_m} increases, the outage probability rises sharply due to increased path loss. However, the rate of performance degradation varies with the value of m: for larger m, corresponding to more favorable channel conditions or a stronger link, the system demonstrates greater resilience to distance-related loss. This suggests that deploying RIS closer to the BS can significantly enhance reliability, especially in weak channel scenarios, and highlights the importance of strategically optimizing RIS placement in practical system design.

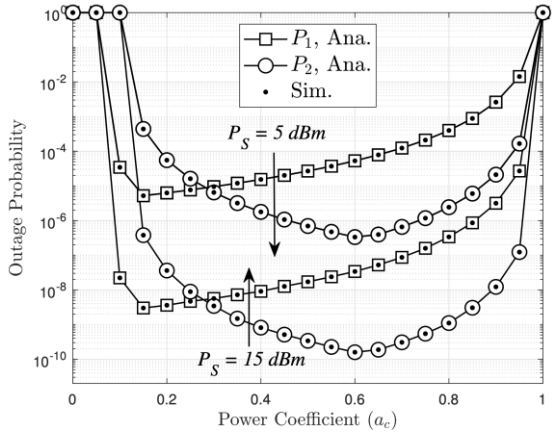

Figure 5. Outage probability versus PA coefficient a_c ($N = M = 2, m = 1$)

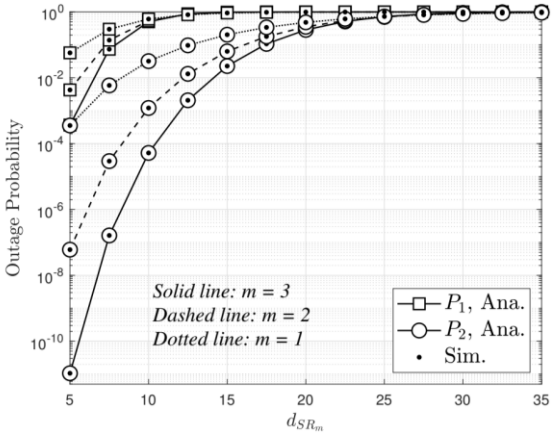

Figure 6. Outage probability versus distance from BS to RISm ($N = 3, M = 2, P_S$ = -15 dBm)

Finally, Figure 7 presents the throughput performance of RSMA and NOMA systems as a function of the BS transmission power (P_S). It is observed that throughput increases with P_S for both systems, with RSMA achieving slightly better performance than NOMA, especially in the low-to-moderate power region. This improvement highlights RSMA's superior ability to manage interference and allocate power efficiently. The analytical and simulation results closely match, confirming the accuracy of the theoretical model. Combined with the outage probability analysis from the previous figure, RSMA demonstrates enhanced reliability and spectral efficiency compared to NOMA.

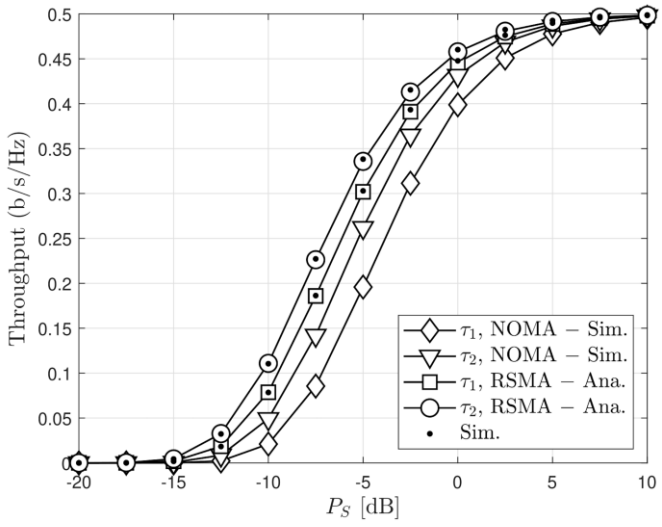

Figure 7. Throughput versus P_S for RSMA and NOMA ($M = 4, N = 2, m = 1$)

For benchmarking, we also compared the proposed RSMA+PRIS scheme against two alternative setups: i) RSMA with full RIS activation and ii) NOMA with PRIS. These additional comparisons confirm that RSMA itself brings significant multi-user interference management gains, while PRIS further reduces overhead and preserves most of the performance of full RIS activation. For completeness, we also evaluated Jain's fairness index under varying PA factors. The results confirm that PRIS-aided RSMA consistently achieves higher fairness compared with conventional NOMA, particularly in low-to-moderate SNR regimes.

In summary, the numerical results confirm the analytical and asymptotic findings and reveal several key trends. Increasing the number of reflecting elements (N) and RISs (M) significantly improves outage performance, while optimal PA (a_c) and strategic RIS placement are critical to enhancing system reliability. Moreover, RSMA demonstrates consistent throughput advantages over NOMA, especially at low-to-moderate transmit power levels. These insights provide practical guidelines for deploying RIS-aided RSMA systems efficiently.

Finally, from a deployment perspective, practical urban scenarios may only accommodate a limited number of RIS panels (e.g., two to four), owing to installation cost, control overhead, and site availability. This aligns with our complexity analysis in section 3.4, highlighting that PRIS is particularly suitable for scalable and cost-effective deployments in dense environments.

5. CONCLUSION

In this study, we investigated the outage probability and throughput performance of RSMA frameworks in a multi-relay radio network system enhanced with RIS technology. We derived closed-form expressions for both outage probability and achievable throughput for each user, considering (i.n.i.d.) Nakagami-m small-scale fading channels. The impact of the PA coefficient was thoroughly analyzed, emphasizing its critical role in optimizing overall system throughput. Notably, the outage performance of user D_2 consistently outperforms that of user D_1. Our results reveal that lower source transmit power P_S leads to higher outage probabilities, whereas increasing P_S effectively reduces outage. Additionally, as system throughput improves, the rates R_1 and R_2 tend to converge. The numerical results confirm that the analytical expressions align well with Monte Carlo simulations over all considered system parameters. Our results suggest that RSMA with PRIS offers a scalable and efficient solution for next-generation wireless systems, particularly in dense urban environments where low-cost and energy-efficient deployments are essential. For future work, it would be valuable to extend this analysis to scenarios involving multiple antennas at the BS, which could further enhance system performance.

ACKNOWLEDGMENTS

This work is a part of the research project CS2025.A4.012 funded by Saigon University.

FUNDING INFORMATION

The authors would like to express their gratitude to Saigon University for providing the financial resources and facilities necessary to conduct this study. This work is a part of the research project CS2025.A4.012 funded by Saigon University.

AUTHOR CONTRIBUTIONS STATEMENT

This journal uses the Contributor Roles Taxonomy (CRediT) to recognize individual author contributions, reduce authorship disputes, and facilitate collaboration.

Name of Author	C	M	So	Va	Fo	I	R	D	O	E	Vi	Su	P	Fu
Hong-Nhu Nguyen					✓				✓					✓
Xuan-Tien Nguyen						✓				✓				
Sang-Quang Nguyen	✓								✓				✓	

C : **C**onceptualization
M : **M**ethodology
So : **So**ftware
Va : **Va**lidation
Fo : **Fo**rmal analysis
I : **I**nvestigation
R : **R**esources
D : **D**ata Curation
O : Writing - **O**riginal Draft
E : Writing - Review & **E**diting
Vi : **Vi**sualization
Su : **Su**pervision
P : **P**roject administration
Fu : **Fu**nding acquisition

CONFLICT OF INTEREST STATEMENT

Authors state no conflict of interest.

DATA AVAILABILITY

This study is based on analytical derivations and numerical simulations. No new datasets were generated or collected

REFERENCES

[1] C.-B. Le, D.-T. Do, X. Li, Y.-F. Huang, H.-C. Chen, and M. Voznak, "Enabling NOMA in Backscatter Reconfigurable Intelligent Surfaces-Aided Systems," *IEEE Access*, vol. 9, pp. 33782–33795, 2021, doi: 10.1109/access.2021.3061429.

[2] W. Saad, M. Bennis, and M. Chen, "A Vision of 6G Wireless Systems: Applications, Trends, Technologies, and Open Research Problems," *IEEE Network*, vol. 34, no. 3, pp. 134–142, May 2020, doi: 10.1109/mnet.001.1900287.

[3] S. Dang, O. Amin, B. Shihada, and M.-S. Alouini, "What should 6G be?," *Nature Electronics*, vol. 3, no. 1, pp. 20–29, Jan. 2020, doi: 10.1038/s41928-019-0355-6.

[4] Q. Wu and R. Zhang, "Towards Smart and Reconfigurable Environment: Intelligent Reflecting Surface Aided Wireless Network," *IEEE Communications Magazine*, vol. 58, no. 1, pp. 106–112, Jan. 2020, doi: 10.1109/mcom.001.1900107.

[5] M. Di Renzo *et al.*, "Smart Radio Environments Empowered by Reconfigurable Intelligent Surfaces: How It Works, State of Research, and The Road Ahead," *IEEE Journal on Selected Areas in Communications*, vol. 38, no. 11, pp. 2450–2525, Nov. 2020, doi: 10.1109/jsac.2020.3007211.

[6] A.-T. Le, T. D. Hieu, T. N. Nguyen, T.-L. Le, S. Q. Nguyen, and M. Voznak, "Physical layer security analysis for RIS-aided NOMA systems with non-colluding eavesdroppers," *Computer Communications*, vol. 219, pp. 194–203, Apr. 2024, doi: 10.1016/j.comcom.2024.03.011.

[7] S.-Q. Nguyen *et al.*, "Statistical Analysis of the Sum of Double Random Variables for Security Applications in RIS-Assisted NOMA Networks with a Direct Link," *Electronics*, vol. 14, no. 2, p. 392, Jan. 2025, doi: 10.3390/electronics14020392.

[8] Q. Wu, S. Zhang, B. Zheng, C. You, and R. Zhang, "Intelligent Reflecting Surface-Aided Wireless Communications: A Tutorial," *IEEE Transactions on Communications*, vol. 69, no. 5, pp. 3313–3351, May 2021, doi: 10.1109/tcomm.2021.3051897.

[9] X. Peng, X. Hu, and C. Zhong, "Distributed Intelligent Reflecting Surfaces-Aided Communication System: Analysis and Design," *IEEE Transactions on Green Communications and Networking*, vol. 6, no. 4, pp. 1932–1944, Dec. 2022, doi: 10.1109/tgcn.2022.3186543.

[10] S. Q. Nguyen, A.-T. Le, V.-D. Phan, H. T. Thien, and R. KhareL, "Outage Performance Analysis of STAR-RIS-NOMA Networks under Imperfect CSI," *Advances in Electrical and Electronic Engineering*, vol. 22, no. 3, Sept. 2024, doi: 10.15598/aeee.v22i3.5546.

[11] C. Huang *et al.*, "Holographic MIMO Surfaces for 6G Wireless Networks: Opportunities, Challenges, and Trends," *IEEE Wireless Communications*, vol. 27, no. 5, pp. 118–125, Oct. 2020, doi: 10.1109/mwc.001.1900534.

[12] Y. Mao, B. Clerckx, and V. O. K. Li, "Rate-splitting multiple access for downlink communication systems: bridging, generalizing, and outperforming SDMA and NOMA," *EURASIP Journal on Wireless Communications and Networking*, vol. 2018, no. 1, May 2018, doi: 10.1186/s13638-018-1104-7.

[13] H. Joudeh and B. Clerckx, "Sum-Rate Maximization for Linearly Precoded Downlink Multiuser MISO Systems With Partial CSIT: A Rate-Splitting Approach," *IEEE Transactions on Communications*, vol. 64, no. 11, pp. 4847–4861, Nov. 2016, doi: 10.1109/tcomm.2016.2603991.

[14] A. Bansal, K. Singh, B. Clerckx, C.-P. Li, and M.-S. Alouini, "Rate-Splitting Multiple Access for Intelligent Reflecting Surface Aided Multi-User Communications," *IEEE Transactions on Vehicular Technology*, vol. 70, no. 9, pp. 9217–9229, Sept. 2021, doi: 10.1109/tvt.2021.3102212.

[15] S. K. Singh, K. Agrawal, K. Singh, B. Clerckx, and C.-P. Li, "RSMA for Hybrid RIS-UAV-Aided Full-Duplex Communications With Finite Blocklength Codes Under Imperfect SIC," *IEEE Transactions on Wireless Communications*, vol. 22, no. 9, pp. 5957–5975, Sept. 2023, doi: 10.1109/twc.2023.3238808.

[16] Y. Ni, H. Zhao, Y. Liu, J. Wang, G. Gui, and H. Zhang, "Analysis of RIS-Aided Communications Over Nakagami-m Fading Channels," *IEEE Transactions on Vehicular Technology*, vol. 72, no. 7, pp. 8709–8721, Jul. 2023, doi: 10.1109/tvt.2023.3234643.

[17] M. Song, X. Yue, C. Ouyang, Y. Liu, T. Li, and T. Hou, "Outage Performance of Active RIS in NOMA Networks over Nakagami-m Fading Channels," in *2023 IEEE 98th Vehicular Technology Conference (VTC2023-Fall)*, IEEE, Oct. 2023, pp. 1–6, doi: 10.1109/vtc2023-fall60731.2023.10333805.

[18] A.-T. Le *et al.*, "Performance Analysis of RIS-Assisted Ambient Backscatter Communication Systems," *IEEE Wireless Communications Letters*, vol. 13, no. 3, pp. 791–795, Mar. 2024, doi: 10.1109/lwc.2023.3344113.

[19] T. N. Do, G. Kaddoum, T. L. Nguyen, D. B. da Costa, and Z. J. Haas, "Multi-RIS-Aided Wireless Systems: Statistical Characterization and Performance Analysis," *IEEE Transactions on Communications*, vol. 69, no. 12, pp. 8641–8658, Dec. 2021, doi: 10.1109/tcomm.2021.3117599.

[20] N. Q. Sang *et al.*, "Performance of RIS-Secured Short-Packet NOMA Systems With Discrete Phase-Shifter to Protect Digital Content and Copyright Against Untrusted User," *IEEE Access*, vol. 13, pp. 21580–21593, 2025, doi: 10.1109/access.2025.3535813.

[21] E. Basar, M. Di Renzo, J. De Rosny, M. Debbah, M.-S. Alouini, and R. Zhang, "Wireless Communications Through Reconfigurable Intelligent Surfaces," *IEEE Access*, vol. 7, pp. 116753–116773, 2019, doi: 10.1109/access.2019.2935192.

[22] T.-H. Vu, D. B. Da Costa, B. V. N. Quoc, and S. Kim, "A Novel Paradigm Shift for Next-Generation: Symbiotic Backscatter Rate-Splitting Multiple Access Systems," in *2024 Tenth International Conference on Communications and Electronics (ICCE)*, IEEE, July 2024, pp. 724–728, doi: 10.1109/icce62051.2024.10634646.

[23] S. Atapattu, R. Fan, P. Dharmawansa, G. Wang, J. Evans, and T. A. Tsiftsis, "Reconfigurable Intelligent Surface Assisted Two–Way Communications: Performance Analysis and Optimization," *IEEE Transactions on Communications*, vol. 68, no. 10, pp. 6552–6567, Oct. 2020, doi: 10.1109/tcomm.2020.3008402.

[24] E. Bjornson, O. Ozdogan, and E. G. Larsson, "Intelligent Reflecting Surface Versus Decode-and-Forward: How Large Surfaces are Needed to Beat Relaying?," *IEEE Wireless Communications Letters*, vol. 9, no. 2, pp. 244–248, Feb. 2020, doi: 10.1109/lwc.2019.2950624.
[25] B. C. Nguyen, L. T. Dung, T. M. Hoang, N. V. Vinh, and G. T. Luu, "On performance of multi-RIS assisted multi-user nonorthogonal multiple access system over Nakagami-m fading channels," *Computer Communications*, vol. 197, pp. 294–305, Jan. 2023, doi: 10.1016/j.comcom.2022.11.010.
[26] D.-T. Do, C.-B. Le, A. Vahid, and S. Mumtaz, "Antenna Selection and Device Grouping for Spectrum-Efficient UAV-Assisted IoT Systems," *IEEE Internet of Things Journal*, vol. 10, no. 9, pp. 8014–8030, May 2023, doi: 10.1109/jiot.2022.3229592.
[27] I. S. Gradshteyn and I. M. Ryzhik, *Table of Integrals, Series, and Products*. Academic Press, 2014.

BIOGRAPHIES OF AUTHORS

Hong-Nhu Nguyen received a B.Sc. in Electronics Engineering from Ho Chi Minh City University of Technology in 1998 and an M.Sc. in Electronics Engineering from the University of Transport and Communications (Vietnam) in 2012. He is currently working as a lecturer at Saigon University, Ho Chi Minh City, Vietnam. He received a Ph.D. in communication technology from the Faculty of Electrical Engineering and Computer Science at VSB - Technical University of Ostrava, Czech Republic in 2021. His research interest includes applied electronics, wireless communications, cognitive radio, NOMA, and energy harvesting. He can be contacted at email: nhu.nh@sgu.edu.vn.

Xuan-Tien Nguyen was born in 1965, received a Bachelor of Physics Specialization in Nuclear Electronics from Dalat University in 1988, and a Master's Degree in Mechatronics Engineering from the University City of Technology. Ho Chi Minh City in 2014. Currently, he is a lecturer in the Department of Electrical-Electronics, Faculty of Electronics and Telecommunications of Saigon University. The field of research now controls robots, mechatronics systems and applications, and machine control methods. He can be contacted at email: tien.nx@sgu.edu.vn.

Dr. Sang-Quang Nguyen received the B.E. degree in Electrical Engineering from Ho Chi Minh City University of Transport, Vietnam, in 2010, the M.E. degree in Telecommunications Engineering from Ho Chi Minh City University of Technology, Vietnam, in 2013, and the Ph.D. degree in Electrical Engineering from the University of Ulsan, South Korea, in 2017. From 2017 to 2021, he was a Lecturer at Duy Tan University, Vietnam. Since May 2021, he has been a Lecturer at Ho Chi Minh City University of Transport, Vietnam. In September 2024, he joined the Post and Telecommunications Institute of Technology, Ho Chi Minh City, as a Lecturer. He also served as a Research Fellow at Queen's University Belfast, United Kingdom, where he contributed to advancements in wireless communications. His research interests include cooperative communications, cognitive radio networks, physical layer security, non-orthogonal multiple access (NOMA), short-packet communications, and backscatter communications. His work primarily focuses on secure and energy-efficient communication solutions for next-generation wireless networks. He can be contacted at email: sangnq@ptit.edu.vn.